HELICAL WIGGLER MODEL FOR FAST TRACKING

W. F. Bergan[†], V. Khachatryan, and D. L. Rubin, Cornell University, Ithaca, NY, USA

Abstract

In order to test the process of Optical Stochastic Cooling (OSC) at the Cornell Electron Storage Ring (CESR), we plan to use helical wigglers as both the pickup and kicker, since the required radiation wavelength of 800nm can be achieved with lower magnetic field strength in helical as compared to planar wigglers. In order to simulate the lattice with such wigglers, it is useful to be able to model the effect of the wiggler on the optics without resorting to direct tracking, which is time-consuming and so ill-suited for the repeated evaluations necessary in running an optimizer. We generate a Taylor map to third order for this element using analytic field expressions, enabling easy determination of the effects of such an element on linear and nonlinear optics. This model is compared with the results of direct tracking and shows good agreement.

INTRODUCTION

Optical stochastic cooling (OSC) is a proposed method to cool particle beams by using the radiation they emit in one wiggler to provide an appropriate energy kick in a second wiggler. Details of the process and plans for a test at the Cornell Electron Storage Ring (CESR) are available in [1]. One important consideration is the wiggler to use. The wavelength of radiation provided by a planar wiggler is given by $\lambda = \frac{\lambda_w}{2\gamma^2}(1 + K^2/2)$, where λ_w is the wiggler period, γ is the relativistic factor, and $K \equiv \frac{eB\lambda_w}{2\pi mc}$ is the undulator parameter, with B being the peak magnetic field, e the electron charge, and m the electron mass. For a helical wiggler, the formula becomes $\lambda = \frac{\lambda_w}{2\gamma^2}(1 + K^2)$. We plan to perform this test with 1 GeV electrons due to difficulties in operating CESR at lower energy. We would also like to obtain radiation at 800 nm, since high-quality light optics are readily available at this wavelength and the radiation may be amplified with a Titanium-sapphire amplifier [2]. In order to meet both these requirements, we need a long wiggler period, and/or a large undulator parameter. Comparing the formulas for the planar and helical wigglers, one can see that the helical wiggler provides the same radiation wavelength with a $\sqrt{2}$ reduction in the strength of the field, reducing the wiggler's effects on beam optics and emittance. Moreover, using a helical wiggler increases the damping provided to the electrons by the OSC process, since the dot product of the radiation's electric field with the electron's velocity is roughly constant along the wiggler, rather than oscillating. We have therefore decided to use helical wigglers with 14 periods of length $\lambda = 32.5$ cm and peak field $B = 0.139$ T, giving an undualtor parameter $K = 4.23$.

In designing a lattice for testing OSC at CESR, it is necessary to optimize various aspects of the linear and nonlinear optics in order to obtain significant cooling rates and acceptances from the OSC process while maintaining good Courant-Snyder parameters and a dynamic aperture which enables us to inject and store a beam. For these repeated optimizations of our lattice, it is useful to have a helical wiggler model which is fast to track through and provides accurate measures of optics through third order so that we can extract amplitude-dependent tune shifts in addition to the effects on the linear optics. At the cost of not having precise information within the wiggler itself, we may compute a map translating initial phase space coordinates of a particle at the wiggler entrance to coordinates at its exit. This map may be formed by dividing the wiggler into thin slices, obtaining maps for these individually, and then concatenating them. For this work, we have used analytic formulas for the field inside a helical undualtor as provided by [3]. This method can be trivially extended to the case where analytic fields are obtained by other methods, as in [4]. Although sufficiently small steps in creating the map will give a result which is near-symplectic, a final symplectification of the map may be performed if desired. This initial work to obtain the map only needs to be completed once for a given wiggler model, and subsequent tracking with it is very fast, as we need only multiply the initial particle phase space coordinates by the terms in the map and sum the results.

CREATION OF THE MAP

We require an analytic expression for the magnetic fields in the accelerator element in question. For our case, we use the expansion of the field of a helical wiggler as presented in [3]. This method will also work with Cartesian expansions as generated by the methods of [4], which permits the inclusion of fringe fields and matching sections.

In moving through a wiggler, the ideal particle will move off-axis under the influence of the magnetic field. For what follows, we will use x, v_x, etc. to refer to the deviation of a particle from the oscillatory reference trajectory. We first note that the change in the horizontal velocity v_x of a particle of charge q, mass m and relativistic gamma factor γ after travelling a distance Δz through some magnetic field is

$$\Delta v_x = q(y'B_z - B_y)/(m\gamma)\Delta z \qquad (1)$$

with similar expressions for Δv_y and Δv_z. We are often interested in the momenta x' and y', which have been normalized by v_z, and so can write

$$\Delta x' = \Delta v_x/v_z - \Delta v_z v_x/v_z^2 \qquad (2)$$

so that

MC2: Photon Sources and Electron Accelerators

T15 Undulators and Wigglers

$$\Delta x' = [q(y'B_z - B_y)/(m\gamma v_z) \qquad (3)$$
$$- v_x q(x'B_y - y'B_x)/(m\gamma v_z^2)]\Delta z$$

$$\Delta y' = [q(B_x - x'B_z)/(m\gamma v_z) \qquad (4)$$
$$- v_y q(x'B_y - y'B_x)/(m\gamma v_z^2)]\Delta z$$

These may be Taylor expanded in terms of the initial x, y, x', y', and γ, noting that $v_z = \sqrt{v^2 - v_x^2 - v_y^2}$, with v and γ constant. Combining these expansions with the simple ones for the position coordinates ($\Delta x = x'\Delta z$) enables us to find the elements of the mapping elements M_{ij}, T_{ijk}, and A_{ijkm}, defined so that the final phase space coordinates x_i are mapped from the initial ones by $x_i = M_{ij}x_j + T_{ijk}x_jx_k + A_{ijkm}x_jx_kx_m$, with repeated indices summed over. These matrix elements may be evaluated along the ideal orbit of the particle, with slices Δz chosen sufficiently thin to satisfy our desired precision.

Having obtained the map for two portions of the wiggler (portion 1 preceding portion 2), they may be concatenated as follows:

$$M_{ij} = M_{ik}^2 M_{kj}^1 \qquad (5)$$

$$T_{ijk} = M_{im}^2 T_{mjk}^1 + T_{imn}^2 M_{mj}^1 M_{nk}^1 \qquad (6)$$

$$A_{ijkm} = M_{in}^2 A_{njkm}^1 + A_{inps}^2 M_{nj}^1 M_{pk}^1 M_{sm}^1 \qquad (7)$$
$$+ T_{inp}^2 T_{njk}^1 M_{pm}^1 + T_{inp}^2 M_{nj}^1 T_{pkm}^1$$

In this manner, one may proceed from maps for individual slices of the wiggler to a map of the wiggler as a whole. Due to the periodicity of the element, we may simplify further by obtaining the map for one period in detail, then concatenating it with itself to construct the whole.

RESULTS

For testing this map, we use a first-order Runge-Kutta method to directly track 1 GeV electrons with various offsets in the initial phase space coordinates through one period of a wiggler with period length 32.5 cm and peak field 0.139 T and fit the final phase space coordinates to polynomial functions of the initial ones. The results are shown in Table 1, and indicate good agreement between the direct tracking and our map. The listed errors only take into account errors from the fit to the tracking results, which are expected to dominate errors in the tracking itself. We acknowledge an asymmetry between the x and y terms in both the map and tracking. However, the expected symmetry is broken by the wiggler phase; the field at the front of the wiggler must point in *some* direction. Introducing a $\pi/2$ phase shift switches the identities of the x and y terms, as expected.

MC2: Photon Sources and Electron Accelerators

T15 Undulators and Wigglers

Table 1: Comparison of Select Terms from Map and Fit to Direct Tracking. Lengths are in meters and angles in radians. Errors are only from the fit to the tracking results.

Term	Map	Tracking
M_{11}	1.00	$1.00 \pm 2 \times 10^{-7}$
M_{12}	0.325	$0.325 \pm 2 \times 10^{-7}$
M_{13}	1.90×10^{-5}	$1.88 \times 10^{-5} \pm 10^{-9}$
M_{14}	-4.76×10^{-6}	$-4.76 \times 10^{-6} \pm 3 \times 10^{-12}$
T_{111}	8.96×10^{-3}	$9.07 \times 10^{-3} \pm 10^{-4}$
T_{122}	5.69×10^{-4}	$5.78 \times 10^{-4} \pm 2 \times 10^{-4}$
T_{133}	0.122	$0.122 \pm 8 \times 10^{-7}$
T_{144}	1.33×10^{-4}	$1.34 \times 10^{-4} \pm 2 \times 10^{-9}$
A_{1111}	-8.09×10^{-3}	0.314 ± 0.3
A_{1222}	-4.35×10^{-5}	0.271 ± 0.3
A_{1333}	2.35×10^{-3}	$2.68 \times 10^{-3} \pm 10^{-3}$
A_{1444}	-3.31×10^{-5}	$-3.46 \times 10^{-5} \pm 5 \times 10^{-6}$
M_{21}	-2.83×10^{-4}	$-2.83 \times 10^{-4} \pm 2 \times 10^{-10}$
M_{22}	1.00	$1.00 \pm 2 \times 10^{-7}$
M_{23}	4.15×10^{-9}	$4.03 \times 10^{-9} \pm 6 \times 10^{-11}$
M_{24}	-4.83×10^{-5}	$-4.81 \times 10^{-5} \pm 4 \times 10^{-11}$
T_{211}	1.27×10^{-6}	$1.49 \times 10^{-6} \pm 2 \times 10^{-7}$
T_{222}	-2.91×10^{-3}	$-3.13 \times 10^{-3} \pm 10^{-4}$
T_{233}	1.73×10^{-5}	$1.72 \times 10^{-5} \pm 4 \times 10^{-8}$
T_{244}	-3.97×10^{-2}	$-3.96 \times 10^{-2} \pm 3 \times 10^{-8}$
A_{2111}	-5.03×10^{-2}	$-4.99 \times 10^{-2} \pm 3 \times 10^{-4}$
A_{2222}	-4.30×10^{-4}	0.402 ± 0.3
A_{2333}	2.97×10^{-6}	$9.00 \times 10^{-6} \pm 8 \times 10^{-5}$
A_{2444}	-1.02×10^{-3}	$-1.01 \times 10^{-3} \pm 5 \times 10^{-5}$
M_{31}	1.90×10^{-5}	$1.88 \times 10^{-5} \pm 2 \times 10^{-11}$
M_{32}	4.76×10^{-6}	$4.76 \times 10^{-6} \pm 2 \times 10^{-12}$
M_{33}	1.00	$1.00 \pm 2 \times 10^{-7}$
M_{34}	0.325	$0.325 \pm 2 \times 10^{-7}$
T_{311}	-6.15×10^{-7}	$-5.07 \times 10^{-7} \pm 2 \times 10^{-8}$
T_{322}	1.52×10^{-3}	$1.52 \times 10^{-3} \pm 2 \times 10^{-9}$
T_{333}	1.16×10^{-6}	$-7.07 \times 10^{-11} \pm 2 \times 10^{-4}$
T_{344}	6.85×10^{-4}	$5.78 \times 10^{-4} \pm 2 \times 10^{-4}$
A_{3111}	4.40×10^{-3}	$4.37 \times 10^{-3} \pm 3 \times 10^{-5}$
A_{3222}	2.65×10^{-5}	$2.36 \times 10^{-5} \pm 3 \times 10^{-6}$
A_{3333}	-8.09×10^{-3}	0.113 ± 0.3
A_{3444}	-1.35×10^{-5}	-0.271 ± 0.3
M_{41}	-4.15×10^{-9}	$-4.54 \times 10^{-9} \pm 2 \times 10^{-13}$
M_{42}	1.03×10^{-5}	$1.05 \times 10^{-5} \pm 9 \times 10^{-12}$
M_{43}	-2.83×10^{-4}	$-2.83 \times 10^{-4} \pm 2 \times 10^{-4}$
M_{44}	1.00	$1.00 \pm 7 \times 10^{-5}$
T_{411}	1.73×10^{-6}	$1.89 \times 10^{-6} \pm 2 \times 10^{-10}$
T_{422}	4.21×10^{-3}	$4.20 \times 10^{-3} \pm 7 \times 10^{-9}$
T_{433}	1.04×10^{-5}	$1.08 \times 10^{-5} \pm 2 \times 10^{-7}$
T_{444}	-4.21×10^{-3}	$-4.26 \times 10^{-3} \pm 10^{-4}$
A_{4111}	-7.44×10^{-7}	$-7.42 \times 10^{-7} \pm 3 \times 10^{-7}$
A_{4222}	-1.49×10^{-4}	$-1.44 \times 10^{-4} \pm 10^{-5}$
A_{4333}	-4.31×10^{-2}	$-4.25 \times 10^{-2} \pm 3 \times 10^{-4}$
A_{4444}	-5.86×10^{-4}	-0.347 ± 0.3

We also compared the predictions of direct tracking with tracking using the Taylor map. Plots showing the shift in y' due to initial offsets in the various phase-space coordinates are shown as Fig. 1 - 3. The worst offender gives a deviation of less than one nrad for a one mm initial offset.
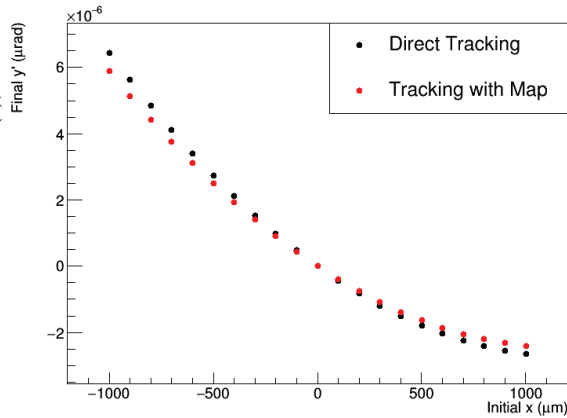

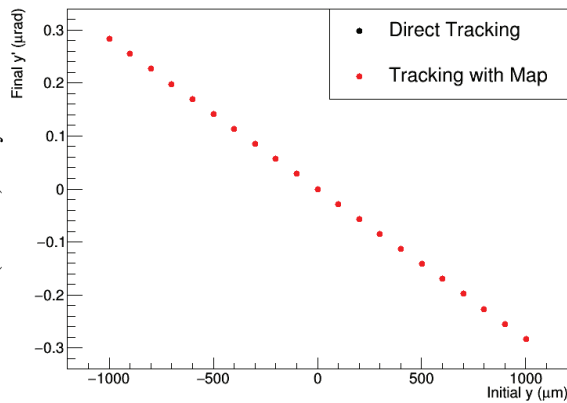Figure 1: Change in final value of y' as a function of initial x offset.

Figure 2: Change in final value of y' as a function of initial y offset.

DISCUSSION

We may compare the terms obtained in this manner with those which appear for a planar wiggler [5]. In the planar case, we expect that the M_{21} term should be equal to $-\frac{(qB)^2 L}{2P^2}$ for a particle of momentum P and charge q moving through a wiggler with peak field B and length L, and that the A_{2111} term should be equal to $-\frac{(qBk_z)^2 L}{3P^2}$ if the wiggler has wavenumber k_z. For our values, these predictions become $M_{21} = -2.83 \times 10^{-4} \text{m}^{-1}$ and $A_{2111} = -7.06 \times 10^{-2} \text{m}^{-3}$. Evidently, the helical wiggler has the same quadrupolar focusing as the planar version. However, the octupolar terms differ, although it is interesting that the sum in quadrature of A_{2111} and A_{4333} comes close to the planar wiggler value.
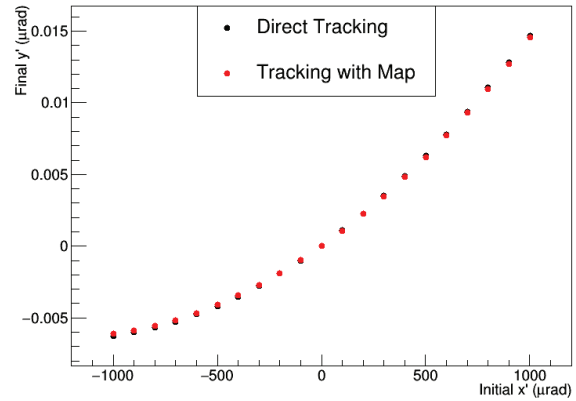

Figure 3: Change in final value of y' as a function of initial x' offset.

RADIATION INTEGRALS

In order to obtain accurate values for the emittance and damping rates, it is necessary to also characterize the energy losses in the wiggler. Fortunately, an examination of the formulas provided in [6] shows that, in the limit as the undulator parameter $K \rightarrow \infty$, the energy losses in the wiggler approach those for a simple dipole. For our case, with $K > 4$, this approximation is better than 1%. It is then sufficient for us to simply evaluate the radiation integrals using the formulas provided in [7], noting that the radius of curvature $\rho = \frac{P}{eB}$ for a particle of momentum P.

CONCLUSIONS

We have generated a map for a helical wiggler using concatenation of Taylor maps for individual slices, enabling fast tracking through a lattice without the need to perform any sort of tracking within the wiggler at run-time. This map agrees well with the results of direct tracking, inspiring confidence in the results obtained using it. The procedure for doing this may be extended to any element where analytic expressions for the fields have been obtained.

FUTURE WORK

So far, we have focused on tracking particles ignoring edge effects; once a design for the wiggler is finalized, we can incorporate edge effects into our map. Additionally, we can apply symplectification techniques at the end of the process to obtain a perfectly symplectic map.

ACKNOWLEDGMENTS

MC2: Photon Sources and Electron Accelerators

T15 Undulators and Wigglers

REFERENCES

[1] W. F. Bergan, M. B. Andorf, M. P. Ehrlichman, V. Khachatryan, D. L. Rubin, and S. Wang, "Bypass design for testing optical stochastic cooling at the Cornell Electron Storage Ring (CESR)", in *Proc. of IPAC'19*, Melbourne, Australia, May 2019, paper MOPGW100, this conference.

[2] A. Zholents and M. Zolotorev, "An amplifier for optical stochastic cooling", in *Proc. of PAC'97*, Vancouver, Canada, May 1997, pp. 1804-1806.

[3] S. H. Kim, "Magnetic field analysis of helical undulators", ANL, Lemont, IL, USA, Rep. ANL/APS/LS-331, 2012.

[4] D, Sagan, J. A. Crittenden, D. Rubin, and E. Forest, "A magnetic field model for wigglers and undulators", in *Proc. of PAC'03*, Portland, OR, USA, May 2003, paper MPPG006, pp. 1023-1025.

[5] J. Corbett and Y. Nosochkov, "Effect of insertion devices in SPEAR-3" in *Proc. of PAC'99*, New York, NY, USA, Mar.-Apr. 1999, pp. 2358-2360.

[6] E.L. Saldin, E.A. Schneidmiller, and M.V. Yurkovb, "Calculation of energy diffusion in an electron beam due to quantum fluctuations of undulator radiation", *Nucl. Instrum. Methods A*, vol. 381, pp. 545-547, 1996.

[7] D. Sagan, "Bmad Reference Manual", `https://www.classe.cornell.edu/bmad/`